Magnetic Navigation for Thoracic Aortic Stent-graft Deployment Using Ultrasound Image Guidance

Zhe Luo, Junfeng Cai, Su Wang, Qiang Zhao, Terry M. Peters, *Fellow, IEEE*, and Lixu Gu*, *Senior Member, IEEE*

***Abstract*—We propose a system for thoracic aortic stent-graft deployment that employs a magnetic tracking system (MTS) and intraoperative ultrasound (US). A preoperative plan is first performed using a general public utilities-accelerated cardiac modeling method to determine the target position of the stent-graft. During the surgery, an MTS is employed to track sensors embedded in the catheter, cannula, and the US probe, while a fiducial landmark based registration is used to map the patient's coordinate to the image coordinate. The surgical target is tracked in real time via a calibrated intraoperative US image. Under the guidance of the MTS integrated with the real-time US images, the stent-graft can be deployed to the target position without the use of ionizing radiation. This navigation approach was validated using both phantom and animal studies. In the phantom study, we demonstrate a US calibration accuracy of 1.5 ± 0.47 mm, and a deployment error of 1.4 ± 0.16 mm. In the animal study, we performed experiments on five porcine subjects and recorded fiducial, target, and deployment errors of 2.5 ± 0.32, 4.2 ± 0.78, and 2.43 ± 0.69 mm, respectively. These results demonstrate that delivery and deployment of thoracic stent-graft under MTS-guided navigation using US imaging is feasible and appropriate for clinical application.**

***Index Terms*—General public utilities (GPU)-accelerated cardiac modeling, magnetic navigation, preoperative planning, ultrasound probe calibration.**

I. Introduction

In 1994, Dake *et al*. [1] first proposed an approach, using endovascular stent-grafts, for the treatment of thoracic aortic aneurysms that employed a customized deployment device to place a stent-graft at the target position of the descending aortic intima under the guidance of X-ray. There has been continuous development of new stent-grafts and implantation techniques over the last ten years, and in 2005, stent-graft was approved for use in the U.S. for the treatment of aneurysms in the thoracic descending aorta [2]. While this approach has subsequently been used widely in other countries including China, fluoroscopy and angiography remain the surgical guidance modality but this has three distinct disadvantages. First, fluoroscopy exposes the clinicians, staff, and patient to ionizing radiation. Second, during the surgery, the patient must be injected with boluses of contrast agent, increasing the risk of iatrogenic renal injury [3]. Third, both fluoroscopy and angiography only provide 2-D images, yielding poor visualization in some regions of the aorta, giving rise to navigational limitations [4].

In recent years, there has been a progressive trend to use MTS in surgical applications [5], [6] to assist in image-guided navigation by providing position and orientation information of instruments and ultrasound transducers. With the ability to relate these devices to the patient coordinate system, preoperative plans and images can be registered to, and combined with, real-time imaging modalities [7]. This approach has the potential to allow the deployment of a stent-graft using ultrasound rather than X-ray guidance. Several researchers have addressed the application of MTS navigation in stent-graft deployment. Wood *et al*. [7] and Levy *et al*. [8] used similar approaches to track wires and catheters in swine during such procedures, while Manstad-Hulaas *et al*. [9] employed navigation technology to deploy stent-grafts for treatment of side-branched abdominal aortic aneurysms in phantoms. Abi-Jaoudeh *et al*. [10] performed a study on three swines using MTS navigation alone for thoracic stent-graft deployment and presented an analysis of accuracy and feasibility. The MTS can show the 3-D information such as the model of instrument and cardiac structure. The relative position between the instrument and patient can be displayed intuitively by using the MTS. However, the MTS alone cannot recover movements of soft tissue during the surgery that could be used to update the preoperative cardiac model.

Intraoperative ultrasound is an attractive complement to preoperative computer tomography (CT)-MRI during surgery with increasing safety, lower cost, ease of use [11]. Real-time US imaging can provide information relating to the surgical target region in real time, leading some researchers to use US imaging in their clinical navigation systems. Huber *et al*. [12] reported the use of US in an animal model of simultaneous intracardiac and intravascular US to navigate an off-pump aortic valve stent implantation. Linte *et al*. [13] developed a navigation system and introduced the US image into the system to construct an augmented reality guidance environment for off-pump, closed, and

Manuscript received March 9, 2012; revised May 16, 2012; accepted June 23, 2012. Date of publication July 6, 2012; date of current version March 7, 2013. This work was supported in part by the the National Natural Science Foundation of China research fund under Grant 61190120 and Grant 61190124 and in part by the Shanghai Municipal Health Bureau research fund under Grant 2011216. *Asterisk indicates corresponding author.*

Z. Luo is with the Image Guided Surgery and Therapy Laboratory, School of Biomedical Engineering, Shanghai Jiao Tong University, Shanghai 200030, China (e-mail: luozhe2007@sjtu.edu.cn).

J. Cai, S. Wang, and Q. Zhao are with the Department of Cardiosurgery, Ruijin Hospital, Shanghai Jiao Tong University, Shanghai 200030, China (e-mail: lonlon_cn@hotmail.com; wangsu1985@gmail.com; zq11607@rjh.com.cn).

T. M. Peters is with the Imaging Research Laboratories, Robarts Research Institute, London, ON, N6A 5K8, Canada (e-mail: tpeters@robarts.ca).

*L. Gu is with the Image Guided Surgery and Therapy Laboratory, School of Biomedical Engineering, Shanghai Jiao Tong University, Shanghai 200030, China (e-mail: gulixu@sjtu.edu.cn).

Color versions of one or more of the figures in this paper are available online at http://ieeexplore.ieee.org.

Digital Object Identifier 10.1109/TBME.2012.2206388

beating intracardiac surgery in a phantom. In addition, Huang *et al*. [11] developed the means to register dynamic 2-D and 3-D US to 3-D CT images of the beating heart in both phantoms and animal models.

The approach proposed in this paper was to combine MTS navigation with US images for the deployment of a stent-graft for treatment of thoracic aortic aneurysms. Here, we replace traditional X-ray guided deployment with MTS tracked US. We first, construct a 3-D cardiac volume model from a preoperative 3-D CT image to allow preoperative planning. Under MTS guidance, the real-time US image can be combined with the preoperative model to assist the surgeon to confidently place the stent-graft on target. We believe that this is the first application of thoracic aortic stent-graft deployment using US imaging assisted by MTS.

II. Materials and Methods

A. General Public Utilities-Accelerated Cardiac Model

The first component of our system is the cardiac model constructed from the patient's preoperative CT images. The CT images were then rendered by a General Public Utilities (GPU)-accelerated raycasting algorithm [14]–[16], implemented with compute unified device architecture programming.

Segmentation of the heart and aorta from the preoperative CT image was achieved via an automatic segmentation algorithm [17], [18] used to first isolate the descending aorta, followed by multistage 3-D image segmentation [19] to isolate the heart. This method consists of two steps. First, seeds are selected manually in the region of the heart to perform a fast matching to delineate an initial contour, which may not contain the entire heart but avoids the leaking caused by introducing global information regarding the contour into the speed function. A morphological reconstruction algorithm was then applied to recover any lost structure from the last stage to achieve whole heart region. Finally, an interactive procedure was employed to separate the resulting segmentation from possibly included surrounding regions. This entire procedure takes seconds for the automatic portion, and less than 4 min for the manual component, making it considerably more efficient than a traditional manual-based segmentation. The segmentation result is displayed using the GPU-accelerated volume rendering procedure, to reconstruct the model shown in Fig. 1.

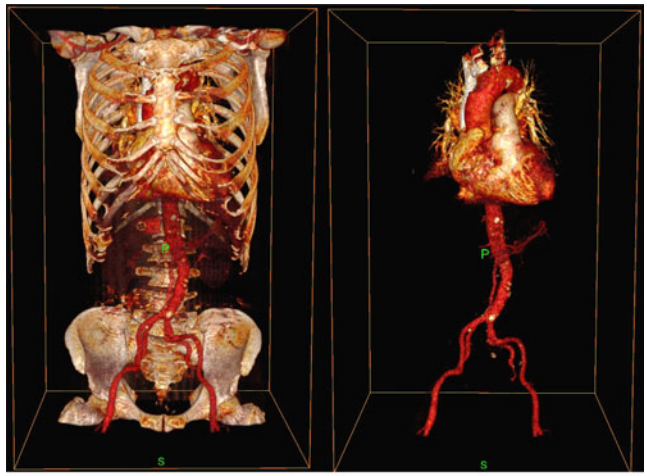

Fig. 1. GPU-accelerated cardiac modeling. (a) GPU-accelerated raycasting volume rendering. (b) Result of GPU-accelerated cardiac modeling.

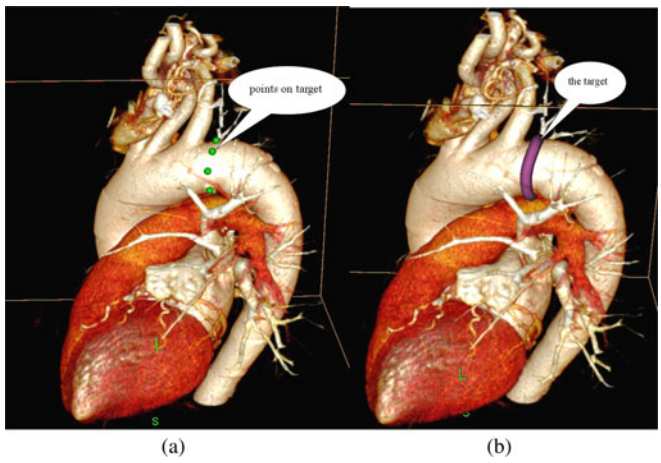

Fig. 2. Preoperative planning. (a) Points on the target. (b) Created target plane. The surgeon analyses the segmented preoperative CT volume to locate the aneurysm (target position) and place some points on the circumference of the vessel at the location of the aneurysm and close to the arteries on the aorta arch. These points define a target plane.

B. Preoperative Planning

Since the unfolded stent-graft is similar to a cylinder, the deployment target can be considered as a plane where the top of the stent-graft should be positioned. Since the intersection of the target plane and the aorta is approximately a circle, the task of preoperative planning is to find the plane (circle) at the disruption of the descending aortic intima.

The target plane is defined on the 3-D heart model by selecting a set of points $p_1, p_2, \ldots, p_n$ evenly distributed on the circumference [see Fig. 2(a)] of the edge of vessel at the location of the aneurysm, and closest to the arteries emanating from the aorta arch. Finally, a least-square fitting algorithm is employed to create a plane of intersection with the aortic arch.

After the target plane is defined, we project these points on the plane to obtain another group of points $p'_1, p'_2, \ldots, p'_n$ as control points to create a cardinal spline to represent the target position circle (the cross section between the target plane and the aorta) as shown in Fig. 2(b).

C. US Probe Calibration

Prior to the use of US in a navigation system, the US probe must be calibrated to determine the transformation from the US image coordinate system to that of the MTS tracking sensor attached to the probe. Fig. 3 shows the various coordinate systems involved in the probe calibration. $TM_{\mathrm{td}\leftarrow\mathrm{ui}}$ is the transform matrix from the US image coordinate system to that of the tracking device, and the $TM_{w\leftarrow\mathrm{td}}$ is the transform relating the tracking device to the world coordinates defined by the MTS. A point in

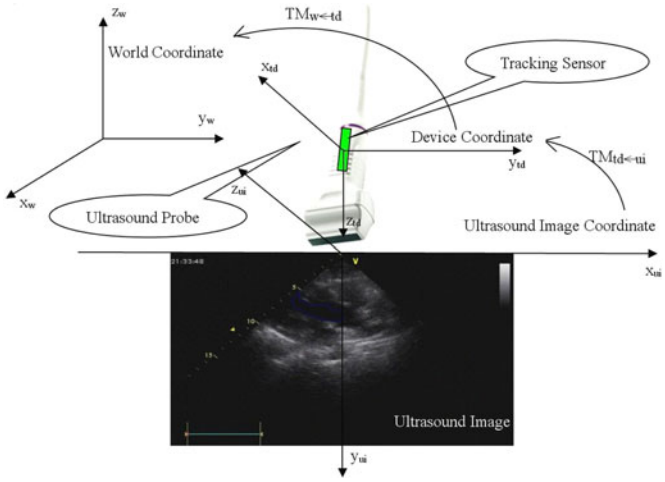

Fig. 3. Coordinates involved in ultrasound probe calibration.

the US image transformed to the world coordinate system can be represented by

$$\begin{pmatrix} x_w \\ y_w \\ z_w \\ 1 \end{pmatrix} = TM_{w\leftarrow \mathrm{td}} \cdot TM_{\mathrm{td}\leftarrow \mathrm{ui}} \begin{pmatrix} s_x \cdot u_x \\ s_y \cdot u_v \\ 0 \\ 1 \end{pmatrix} \tag{1}$$

where (u_k, u_v) represents a point in the US image, s_x, s_y are the scale factors of the x and y axes, respectively, and (x_w, y_w, z_w) is the corresponding location in world coordinates.

Because of the speed necessary to perform the US calibration in the operating room, we chose a 2-D alignment method [20], [21] to calibrate the probe.

D. Calibration Phantom

The basic idea of 2-D alignment is to manually align the US plane with a set of points [22]. We designed and built a customized calibration phantom comprising a box with in which a calibration panel containing 25 polyvinylchloride cylinders of 1.5-mm radius and 1-mm height is placed for this purpose (Fig. 4). Each cylinder contains a 0.5-mm divot within its exposed surface, and is inserted into the panel in 1-mm deep holes.

E. Automatic Detection and Identification of Image Points

We developed an automatic algorithm to detect the centers of cylinders in the US image, when the US image plane is aligned with the plane defined by the centers of the cylinders.

Since the intensity of the cylinders in US image is much higher than that of most of the speckle in the images, they may be isolated by using a threshold (in our application, the threshold value is set at 190 on 256 step scale). After thresholding, a morphological opening operation [23] is then performed to remove any spurious points. Because the cross section of the cylinder in the US image plane is approximately disk-shaped, a shape detection technique can be used to detect the cylinders in the US image. Finally, a Hough Transform [24] is used to define the centers.

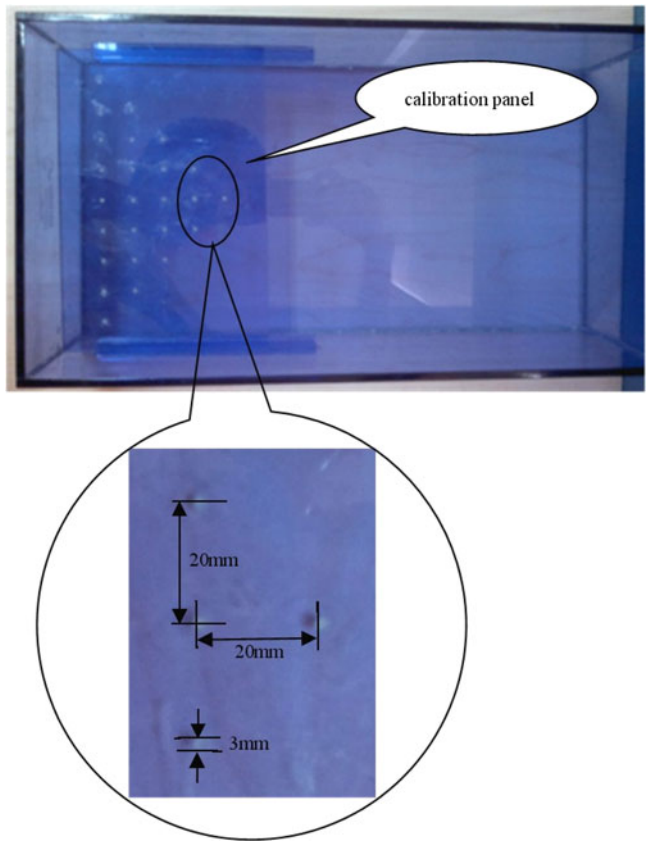

Fig. 4. Box with calibration panel containing 25 cylinders (height:1 mm, radius: 1.5 mm) in a triangular formation.

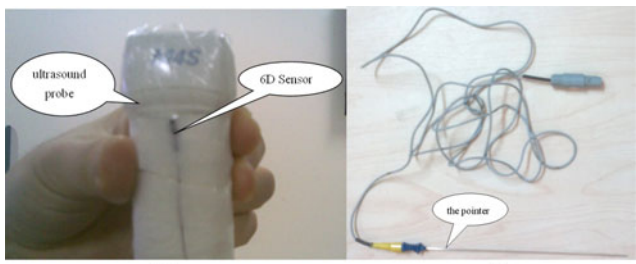

Fig. 5. Tracked devices in probe calibration. (a) Probe to be calibrated with a tracked 6-D sensor. (b) Tracked pointer to catch the real world positions of cylinders.

F. Implementation of Probe Calibration

The probe calibration matrix $TM_{\mathrm{td}\leftarrow \mathrm{ui}}$ is calculated in the following manner:

1) attach a 6-D OFMT sensor to the probe [see Fig. 5(a)];
2) align the calibration phantom with the center of the MTS field generator;
3) fill the calibration phantom with a mixture of water and 10% glycerol at about 20° C;
4) place the US probe into the mixture and adjust its direction and position to align the US plane with the target plane

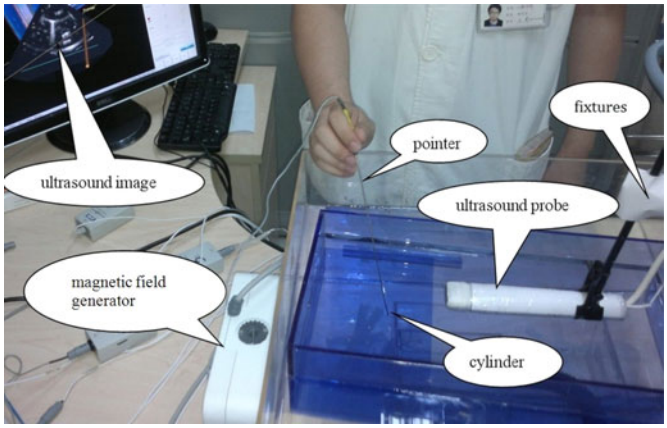

Fig. 6. All the components in a probe calibration scenario.

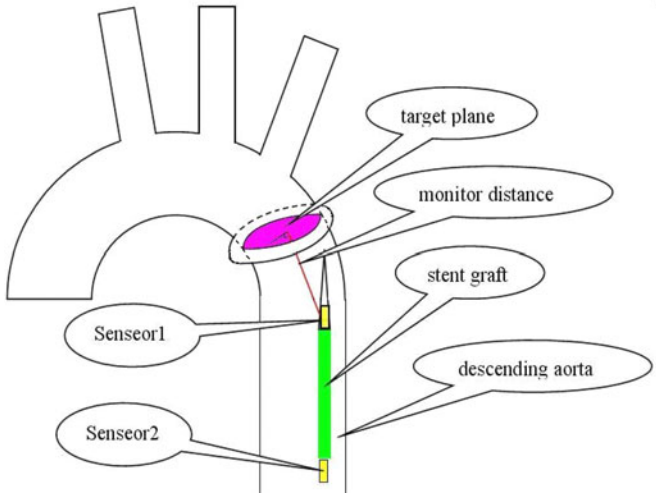

Fig. 7. Distance tracked by electromagnetic navigation system.

Fig. 8. Stent-graft used in this study.

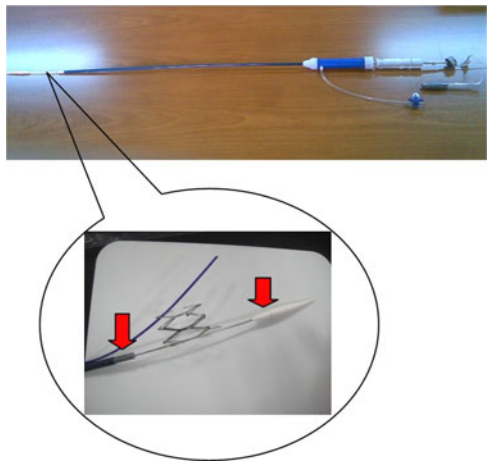

Fig. 9. Catheter used in this study. Two red arrows indicate the location of the sensors.

defined by the centers of the cylinders in the calibration panel;

5) fix the probe in a rigid mount (see Fig. 6);
6) the centers of cylinders are automatically detected with positions $p^j_{\mathrm{ui}}, j = 1, 2 \ldots N$ in US image coordinate system;
7) the positions $p^j_w, j = 1, 2 \ldots N$ of each calibration post are recorded by placing an MTS-tracked pointer tip within the divot on each post [see Fig. 5(b)];
8) a rigid body transformation that minimizes the mean Euclidian distance between the two homologous point sets p^j_{ui} and p^j_w is used to calculate the probe calibration matrix $TM_{\mathrm{td}\leftarrow\mathrm{ui}}$ in (2):

$$TM_{\mathrm{td}\leftarrow\mathrm{ui}} = \arg\min_{TM} \sum_{j=1}^{N} ||TM_{w\leftarrow\mathrm{td}} \cdot TM \cdot p^j_{\mathrm{ui}} - p^j_w|| \tag{2}$$

which is calculated using a direct least-squares error minimization technique [25].

G. Registration

Before implementing real-time tracking, the patient is registered to the images represented within the visualization computer using a rigid, landmark-based transformation that minimizes the mean-squared distance between homologous landmarks in the image and patient. The landmarks we used are the ECG electrodes that are uniformly distributed on the patient's chest.

H. Navigation

Following preoperative planning, US probe calibration and registration, the stent-graft and target plane are displayed in the augmented reality environment of our navigation system (see Fig 7), where the target plane is depicted in pink and the red line segment perpendicular to the target plane represents the distance from the top point of the stent-graft to the target plane. The navigation system monitors this distance and displays it within the virtual image. During the surgery, the sensors provide an intuitive depiction of the orientation and position of the stent-graft within the aorta.

I. Components

1) Stent-Graft: The nitinol stent-graft expands to its final shape at normal temperature, but can be compressed in ice water to fit inside a catheter (see Fig. 8).

2) Catheter: As shown in the Fig. 9, two sensors are placed in the forward section of the catheter. The stent-graft is compressed and embedded between the two sensors so that the MTS

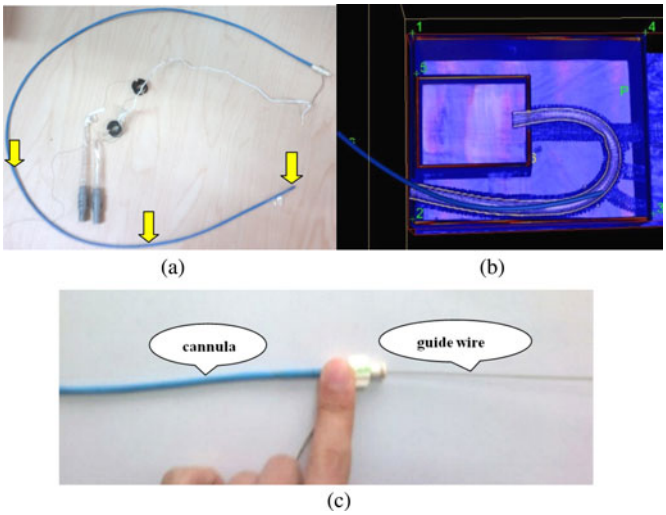

Fig. 10. Guided wire. (a) Three yellow arrows indicate the location of sensors in the cannula. (b) Cannula in the electromagnetic navigation system. (c) Guide wire inserted in the cannula.

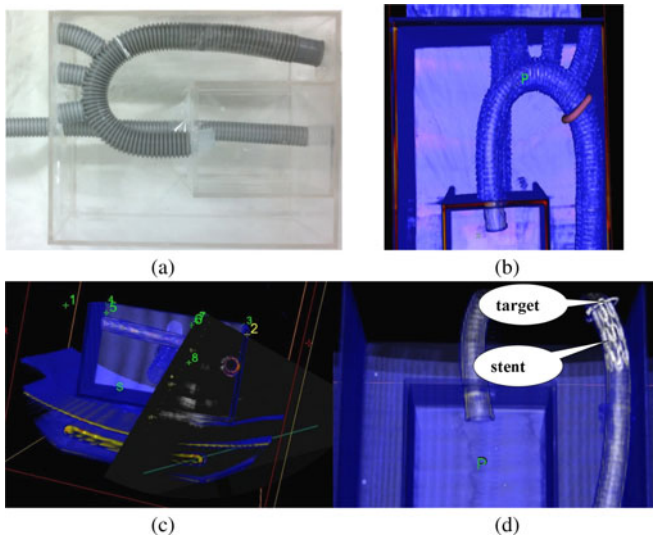

Fig. 11. Phantom study. (a) Phantom. (b) Preoperative planning result of phantom study. (c) Fuse the ultrasound image with preoperative CT model of the phantom. (d) Result of the stent-graft deployment in phantom.

can track the stent-graft when the catheter is inserted into the aorta.

3) Guide Wire and Cannula: Prior to the insertion of the stent, a guide wire is advanced from the common femoral artery access into the aortic arch. The guide wire is enclosed by a cannula in which three MTS sensors are embedded [see Fig. 10(a) and (c)] to enable tracking [see Fig. 10(b)]. A cardinal spline fit to the positions of these three sensors creates a model of the cannula that can be displayed in the virtual reality (VR) environment. When the cannula arrives at the aortic arch, it is extracted, while the guide wire remains to guide the catheter into the aorta.

4) Tracking Device: An Aurora MTS sensor (Northern Digital, Waterloo, ON, Canada) was used to track the pose of both the catheter and the US probe. For US image tracking, a standard 6-DOF sensor coil was mounted onto the US probe [see Fig. 5(a)].

5) Software: Software for this system was developed based on the cardiac navigation platform that we have implemented [26] using Python 2.7, and makes extensive use of classes from the VTK 5.4 (www.vtk.org) and Atamai (www.atamai.com). The system runs under Windows XP, on an Intel Core i5 computer with NVIDIA GeForce GTX 460 graphics card. US images were acquired using a GE Vivid 7 US machine, with the images being integrated into our navigation system after probe calibration.

The system displays the 3-D cardiac model of patient, along with a semitransparent calibrated US image plane to provide an updated interior view of the aorta in real time. The model of the stent-graft is also displayed in the system after insertion into the descending aorta, along with its distance from the target position.

J. Experiments

1) Evaluation of Probe Calibration: To evaluate the probe calibration, we employ a 3-D navigation accuracy measure (3-D NAC) [22] to determine the quality of the calibration. The 3-D NAC compares the transformed points directly to the physically measured coordinates, and is defined as

$$\Delta_{3\mathrm{D\,NAC}} = \underset{j}{\mathrm{mean}}\{||TM_{w\leftarrow \mathrm{td}} \cdot TM_{\mathrm{td}\leftarrow \mathrm{ui}} \cdot p^j_{\mathrm{ui}} - p^j_w||\} \quad (3)$$

where $\Delta_{3\mathrm{DNAC}}$ is the 3-D NAC, $TM_{w\leftarrow \mathrm{td}}$ is the transform from the tracked device (sensor) coordinate system to world coordinates, $TM_{\mathrm{td}\leftarrow \mathrm{ui}}$ is the transform between the US image and the tracked device, while p^j_{ui} and $p^j_w (j = 1, 2 \ldots N)$ are the coordinates of the points in the US world coordinates, respectively.

2) Phantom Study: We first performed a phantom study to verify the feasibility of the navigation system. In the validation experiment, as shown in Fig. 11(a), the heart was represented by a phantom, constructed from transparent plastic. The small cube in the phantom simulates the heart, while the bent tube mimics the descending aorta and the straight tube the esophagus. The corners of the phantom were used as the landmarks for the fiducial marker-based registration.

A volume model and the preoperative plan were constructed from the CT image of the phantom [see Fig. 11(b)]. After the probe calibration and registration were performed, the US image was integrated into the system [see Fig. 11(c)]. When the tracked catheter was inserted into the bent tube (aorta), the system was able to visualize the model of the stent-graft embedded in the distal end of the catheter, and report the distance between the center of stent-graft and the target plane. When the distance shown in the system was close to zero, the catheter was opened to release the stent-graft, which unfolded and could be deployed to the target position.

3) Animal Study: Further validation of the system was achieved using a porcine study that employed valve deployment on five animals. Here, three errors were measured.

1) Fiducial registration error (FRE) was assessed in each case by calculating the root mean square of the difference between the fiducial marker positions in image space and their registered positions in world coordinates [25]. FRE

TABLE I
RESULT OF 3-D NAC

Position	Point1	Point 2	Point3	Point4	Point5	Point6	Point7	Point8	Point9	Point10	Mean
1	1.05	1.12	1.31	2.01	1.58	2.11	1.34	2.07	0.91	1.27	1.48
2	1.40	2.21	0.84	1.83	1.56	1.68	2.16	1.57	2.30	1.08	1.66
3	2.21	0.82	2.15	1.75	0.84	1.26	0.92	2.17	1.38	1.62	1.51
4	1.26	1.01	2.05	0.95	1.33	2.30	1.48	0.88	1.52	1.41	1.42
5	0.86	1.23	1.16	1.59	2.12	0.87	1.20	1.43	2.05	2.01	1.45

is defined as

$$\text{FRE} = \frac{1}{N}\sum_{i=1}^{N} |Tx_i - y_i| \tag{4}$$

where N is the number of source points, and T is the transform between the world coordinates and the preoperative CT image. The fiducial registration algorithm finds the transform T that minimizes the FRE. After registration, the FRE can be reported from our system automatically.

2) Target registration error (TRE) defines the misregistration error between the tracked device location displayed by the system, and its actual location. The TRE is measure by advancing the tracked cannula from the common femoral artery access to the aortic arch after registering the pig's CT image to world coordinates using surface-mounted fiducials. The locations p^i_{navi} of the three sensors were reported by the system. We then fixed the cannula inside the aorta and the postoperative image was acquired. We made the assumption that the positions of fiducial landmarks attached to the pig were unchanged between the preoperative and postoperative images. Since it is fixed by the mediastinal pleura, the aortic arch and the descending aorta can be considered relatively static and rigid; a mutual information registration was employed to refine the registration from the postoperative to the preoperative image to achieve the final transformation TM. Because the sensors can be identified easily in the CT image, their positions p^i_{post} on the cannula in the postoperative image coordinate system were measured and considered as ground truth. We transformed the p^i_{post} by $p^i_{\text{pre}} = TM \cdot p^i_{\text{post}}$, where p^i_{pre} are their positions in the preoperative image coordinate frame. The TRE is then computed by

$$\text{TRE} = \frac{1}{N}\sum_{i=1}^{N} \left|p^i_{\text{pre}} - p^i_{\text{navi}}\right| \tag{5}$$

where N is the number of sensors in the cannula.

3) Deployment error is defined as the difference between actual final stent-graft position and preoperative planning deployment position. After the postoperative and preoperative images were registered, the deployment error was measured as the distance between the leading edge of stent-graft to the target plane in the postoperative CT coordinate system.

In each case, the three measurements were employed to calculate the final errors.

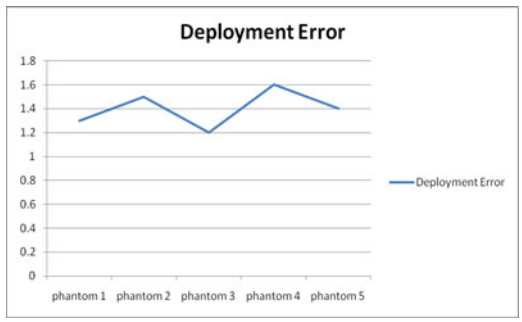

Fig. 12. Deployment error recorded for the phantom study.

III. RESULTS

A. Evaluation of Probe Calibration

After the probe calibration was performed, the calibration panel was used to compute the 3-D NAC by placing it in several positions with different orientations. In each position, the US plane was aligned to the plane defined by the centers of cylinders in the panel. Then, the position of each cylinder center in the US image coordinate was detected by the algorithm described earlier, and the position p^j_w in world space was detected by the tracked pointer. Afterward, all the p^j_{ui} and p^j_w were used as input to (3) to calculate the 3-D NAC.

Table I shows the results of 3-D NAC, demonstrating an average accuracy of 1.5 ± 0.47 mm.

B. Phantom Study

To measure the deployment error, a "postoperative" CT image of the phantom with pixel spacing of 0.64×0.64 and slice thickness of 0.75 mm was acquired so that the actual distance between the stent-graft and the target position could be measured. We performed the phantom experiment five times and recorded each deployment error in the Fig. 12, resulting in an average error of 1.4 ± 0.16 mm.

C. Animal Study

The details of the experiment are as follows.

Pigs weighing between 51 and 60 kg were selected for the experiments. Six fiducial landmarks used for registration were attached on the skin in the area of the rib cage (see Fig. 13). The animals were anesthetized and the heart rate was reduced to 70–90 beats/min by injected Betaloc (5 mg:5 mL, Vetter Pharma-Fertigung Gmbh & CoKG, Germany) during

Fig. 13. Fiducial landmark on a swine chest.

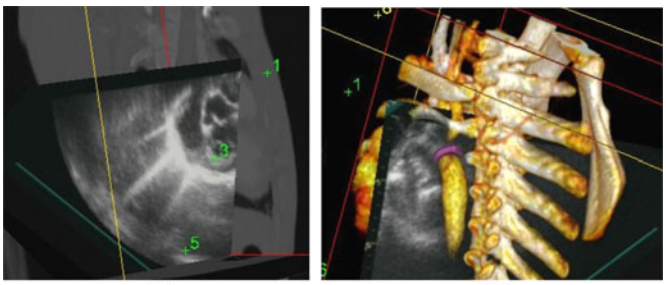

Fig. 14. Real-time ultrasound image fused with preoperative CT model of swine. (a) Fused with a CT image. (b) Fused with the cardiac model.

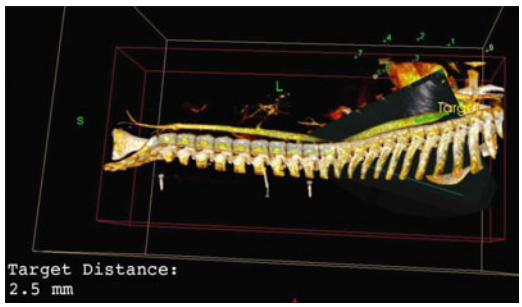

Fig. 15. Guidance of magnetic tracking with the ultrasound image. Target distance is the distance between the stent-graft and the target plane defined before.

the procedure. Respiration was controlled by a mechanical ventilator at 15–20 cycles/min.

The preoperative CT image of the animal with pixel spacing of 0.625×0.625 and slice thickness of 1.25 mm was then imported into the navigation system, where the volume cardiac model was reconstructed using the raycasting algorithm described earlier. Preoperative planning was performed on the model and the target position of the stent-graft was determined.

Finally, the fiducial landmark registration was performed and the calibration of the US probe was achieved using the calibration phantom, the real-time US image fused with the CT image (see Fig. 14), and the tracked guide wire was advanced from the common femoral artery access to the aortic arch. When the cannula arrived at the aortic arch along with the guide wire, the former was removed, allowing the catheter to enter the aorta along the guide wire. Under the guidance of the system and the fused real-time US image (see Fig. 15), the surgeon was able to confidently reach the target position and release the stent-graft

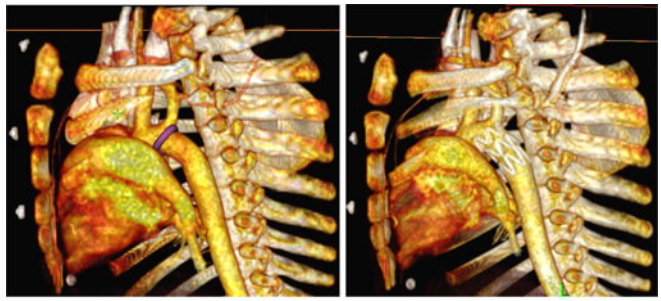

Fig. 16. One of the animal studies. (a) Target. (b) Stent-graft after deployment.

to the correct target. After the operation, the postoperative CT image was examined to determine the deployment error, which was considered to be the actual distance between the position of the stent-graft and the target position. Fig. 16 shows one of the animal experiment results. The FRE is 2.5 ± 0.32 mm, the TRE is 4.2 ± 0.78 mm and the deployment error is 2.43 ± 0.69 mm.

IV. Discussion and Future Work

In the US probe calibration, the US image plane should align with the plane defined by the centers of cylinder in the calibration panel. However, there is an error in this alignment, which in turn introduces errors into the final result. The ultrasound beam profile effect will also have a significant effect here. Similar to the method employed by Sato *et al*. [20] to reduce its effect, the geometric center of the phantom panel is in the ultrasound beam focal range (the ultrasound probe used in this study is multi focal, with a focal range of 10–15 cm) so that the points on the phantom panel easily can be localized in the acquired US image during the US probe calibration procedure. Similar to the fiducial landmark registration, the probe calibration used a pointer whose tip was tracked to obtain its position and orientation in real world space. The orientation and position are calculated according to the tip position relative to the coordinate of the sensor attached in its axis. The error of automatic detection of the center of the cylinder in the US plane is yet another source error.

Although the thoracic aorta deforms due to cardiac and respiratory motion, the rigid registration with fused US image used for endovascular stent-graft procedures is reasonable and feasible, since the deformation of descending aorta is small (the maximum average diameter change of descending aorta between an RR interval is less than 2 mm [26].). The deformation that does need to be compensated for is the slight motion of the aorta arch. Although the MTS may not be sufficiently accurate for this purpose, the real-time US image at this position can compensate for this error. Furthermore, the ventilator controls the respiration to reduce the influence of breathing during the procedure.

Three errors were measured in this research: FRE, TRE, and deployment error. The TRE represents the actual registration error, which is influenced by the selection of fiducials in image and real space, the coregistration between pre- and postoperative images, and respiration, the latter being the main source of error. Respiration error can however be minimized through the use of a ventilator. The deployment error measures the overall

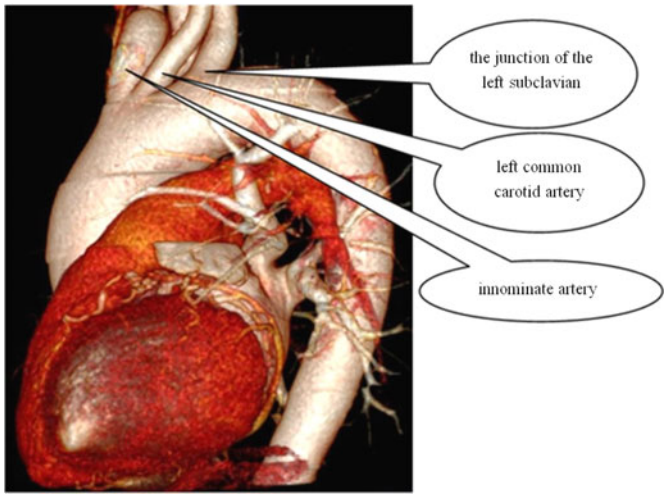

Fig. 17. Junction of the left subclavian, left common carotid artery, and innominate artery.

accuracy of the system, to which the FRE and TRE contribute. However, on the one hand, the 3-D model of heart and aorta in the system are static, while the heart is beating and the aorta is pulsating with the heart. When the stent-graft is guided by system, its reported position will differ slightly from reality because of this effect, increasing the deployment error. On the other hand, when the stent-graft is released, it may slide along the vessel wall, which also can introduce additional deployment error. Although the aorta is pulsating, the effect of pulsation decreases with distance from the heart, and for the most part the descending aorta can be considered as static. When the stent-graft was close to the target position near the aortic arch, the real-time US image was employed to compensate for the error, and to visualize the anatomy of the target region. Thus, following the paradigm introduced by Linte *et al*. [13], the VR system is employed to optimally navigate toward the target, while the real-time imaging modality (US) is employed to guide the final placement.

In addition to the traditional deployment via fluoroscopic guidance, there are three possible methods to deploy the stent-graft, MTS guidance only, US guidance only, and MTS plus US guidance.

For the MTS guidance only, the structure of the descending aorta far from the aortic arch is straight and simple without crucial subvessels, and we believe the virtual model augmented by the MTS-tracked catheter will satisfy clinical needs. Our study mainly focuses on the stent-graft deployment for the aortic arch, in the region of the descending aortic dissection close to the junction of the left subclavian artery. Because the aorta arch is adjacent to the heart, it will move with the beating heart. Because the preoperative image is static, there is no real-time dynamic information relating to the motion of the arch, under MTS-only guidance the placement of the stent-graft could increase the risk of blocking the junction to this branch. MTS guidance alone at the region of the innominate artery, left common carotid artery and the junction of the left subclavian artery (see Fig. 17) on the aorta cannot guarantee accurate placement.

For US guidance only, the intraoperative US image can provide information relating to the surgical target region in real time, allowing the surgeon to determine from the US images whether the position of the stent-graft is likely to block these junctions. However, because of the complexity of the target region and the low quality of US image, US-only navigation may also be difficult for the surgeon to even locate the target region. For patients with a good intercostal acoustic window, the aortic arch and the region close to it can be clearly seen. However, the quality of the US image in regions further from the aortic arch is compromised by the effects of air in the lung. We also attempted five animal cases using only US guidance and all of them failed. In each case, when the stent-graft was in the aorta, affected by the intestine and the lung, the surgeon could hardly trace the stent-graft only by US, especially in the descending aorta area behind the lung, and finally had to give up the procedure.

Our navigation system uses MTS combined with US, and provides a flexible platform for fusing intraoperative US images with preoperative CT image to compensate for the lack of direct vision during deployment of the stent-graft. If the target position is far from the aortic arch, the error of the MTS-guided navigation is probably acceptable. However, when the stent-graft target is close to the aortic arch, it could potentially block the junction of the left subclavian artery, the left common carotid artery and the innominate artery. Here, real-time US guidance plays a significant role in ensuring that the final positioning is appropriate. In our combined navigation system, the orientation of the US image is tracked and fused with the preoperative cardiac model to track the location of the stent-graft in real time. This method comprises two parts, navigation and positioning. "Navigation" guides the stent-graft to the small region that is well visualized in the US image and contains the target position. "Positioning" employs the intraoperative US image to accurately localize the target. The MTS (VR) navigates the stent-graft to target region and then enhances the US. The US enhanced by VR finally positions the target position and guides the placement of stent-graft. With the complementary information captured in two different modalities, the results of our approach are safer, more stable, and clinically applicable.

In a similar study without the use of US, Abi-Jaoudeh *et al*. [10], reported a TRE and deployment error 4.3 ± 0.97 mm and 2.6 ± 3.0 mm, respectively, compared to our average result (TRE: 4.2 ± 0.78 mm, deployment error: 2.43 ± 0.69 mm). While our precision is somewhat improved, given a sample size of three for Abi-Jaoudeh's study and five for our own, we cannot claim that the improvement is significant. However, the use of US offers the opportunity to reregister the target during the procedure.

The phantom and porcine studies reveal that MTS tracking coupled with real-time US image allowed more accurate deployment of the stent-graft near the target position. We acknowledge the potential problems of employing transthoracic imaging in the case of air in the lungs in the ultrasound beam path. An alternative approach (not explicitly addressed in our current work) is the use of transesophageal echo to visualize the aortic arch [28].

While the cardiac model in this paper is static, it is planned in future work to upgrade the model to a dynamic version. To

make better use of the real-time US image, object region contour tracking technique will be introduced to track the contour of the aorta in the low-contrast US images. At that point we plan to validate the procedure in human clinical trials. While this work represents a proof of principle, our final goal is to use an MTS in conjunction with intraoperative US to guide the deployment of stent-graft deployment for aortic valve deployment, where deformation tracking is a challenging issue.

V. Conclusion

This paper proposed an MTS enabled navigation system for thoracic aortic stent-graft deployment using intraoperative US imaging. The phantom and animal study results revealed that this method is feasible and accurate for delivery and deployment of an aortic stent-graft.

References

[1] M. D. Dake, D. C. Miller, C. P. Semba, R. S. Mitchell, P. J. Walker, and R. P. Liddell, "Transluminal placement of endovascular stent-grafts for the treatment of descending thoracic aortic aneurysms," *N. Engl. J. Med.*, vol. 331, no. 26, pp. 1729–1734, Dec. 1994.

[2] L. G. Svensson, N. T. Kouchoukos, D. C. Miller, J. E. Bavaria, J. S. Coselli, M. A. Curi, H. Eggebrencht, J. A. Elefteriades, R. Erbel, T. G. Gleason, B. W. Lytle, R. S. Mitchell, C. A. Nienaber, E. E. Roselli, H. J. Safi, R. J. Shemin, G. A. Sicard, T. M. Sundt 3rd, W. Y. Szeto, and G. H. Wheatley 3rd, "Expert consensus document on the treatment of descending thoracic aortic disease using endovascular stent-grafts," *Ann. Thorac. Surg.*, vol. 85, pp. S1–S41, 2008.

[3] D. Tarek, "An evidence-based approach to minimise contrast-induced neuropathy," *J. New Zealand Med. Assoc.*, vol. 122, pp. 39–41, Jul. 2009.

[4] R. K. Greenberg, S. Haulon, S. O'Neill, S. Lyden, and K. Ouriel, "Primary endovascular repair of juxtarenal aneurysms with fenestrated endovascular grafting," *Eur. J. Vasc. Endovasc. Surg.*, vol. 27, pp. 484–491, May 2004.

[5] J. H. Kaspersen, E. Sjølie, J. Wesche, J. Åsland, J. Lundbom, A. Ødegård, F. Lindseth, and T. A. Nagelhus Hernes, "Three-dimensional ultrasound-based navigation combined with preoperative CT during abdominal interventions: A feasibility study," *Cardiovasc. Intervent. Radiol.*, vol. 26, no. 4, pp. 347–356, 2003.

[6] C. Schichor, K. Schöller, P. Tanner, E. Uhl, R. Goldbrunner, J. C. Tonn, and J. Witte, "Magnetically guided neuro navigation of flexible instruments in shunt placement, transsphenoidal procedures, and craniotomies," *Neurosurgery*, vol. 63, pp. 121–128, Jul. 2008.

[7] B. J. Wood, H. Zhang, A. Durrani, N. Glossop, S. Ranjan, D. Lindisch, E. Levy, F. Banovac, J. Borgert, S. Krueger, and J. Kruecker, "Navigation with electromagnetic tracking for interventional radiology procedures: A feasibility study," *J. Vasc. Intervent. Radiol.*, vol. 16, pp. 493–505, Apr. 2005.

[8] E. B. Levy, H. Zhang, D. Lindisch, B. J. Wood, and K. Cleary, "Electromagnetic tracking-guided percutaneous intrahepatic portosystemic shunt creation in a swine model," *J. Vasc. Intervent. Radiol.*, vol. 18, pp. 303–307, Feb. 2007.

[9] F. Manstad-Hulaas, S. Ommedal, G. A. Tangen, P. Aadahl, and T. N. Hernes, "Sidebranched AAA stent graft insertion using navigation technology: A phantom study," *Eur. Surg. Res.*, vol. 39, no. 6, pp. 364–371, Jul. 2007.

[10] N. Abi-Jaoudeh, N. Glossop, M. Dake, W. F. Pritchard, A. Chiesa, M. R. Dreher, T. Tang, J. W. Karanian, and B. J. Wood, "Electromagnetic navigation for thoracic aortic stent-graft deployment: A pilot study in swine," *J. Vasc. Intervent. Radiol.*, vol. 21, pp. 888–895, Apr. 2010.

[11] X. Huang, J. Moore, G. Guiraudon, D. L. Jones, D. Bainbridge, J. Renand, and T. M. Peters, "Dynamic 2-D ultrasound and 3-D CT image registration of the beating heart," *IEEE Trans. Med. Imag.*, vol. 28, no. 8, pp. 1179–1189, Aug. 2009.

[12] C. H. Huber, M. Nasratulla, M. Augstburger, and L. K. Von Segesser, "Ultrasound navigation through the heart for off-pump aortic valved stent implantation: New tool," *J. Endovasc. Therapy*, vol. 11, pp. 503–510, Aug. 2004.

[13] C. A. Linte, J. Moore, C. Wedlake, and T. M. Peters, "Evaluation of model-enhanced ultrasound-assisted interventional guidance in a cardiac phantom," *IEEE Trans. Biomed. Eng.*, vol. 57, no. 9, pp. 2209–2218, Sep. 2010.

[14] M. Levoy, "Efficient ray tracing of volume data," *ACM Trans. Graph.*, vol. 9, pp. 245–261, 1990.

[15] H. Yang and L. Gu, "GPU-based volume rendering for medical image visualization," in *Proc. 27th Annu. Conf. IEEE Eng. Med. Biol.*, Shanghai, China, 2005, pp. 5145–5148.

[16] T. Lee, J. Lee, H. Lee, H. Kye, Y. Shin, and S. Kim, "Fast perspective volume ray casting method using GPU-based acceleration techniques for translucency rendering in 3-D endoluminal CT colonography," *Comput. Biol. Med.*, vol. 39, pp. 657–666, Aug. 2009.

[17] C. Lorenz, J. Lessick, G. Lavi, T. Bulow, and S. Renisch, "Fast automatic delineation of cardiac volume of interest in MSCT images," in *Proc. SPIE*, San Diego, CA, 2004, pp. 456–466.

[18] S. C. Saur, C. Kühnel, T. Boskamp, G. Székely, and P. Cattin, "Automatic ascending aorta detection in CTA datasets," *Bildverarbeitungfür der Medizin*, vol. 6, pp. 323–327, 2008.

[19] L. Gu, J. Xu, and T. M. Peters, "Novel multistage three-dimensional medical image segmentation: Methodology and validation," *IEEE Trans. Inf. Technol. Biomed.*, vol. 10, no. 4, pp. 740–748, Oct. 2006.

[20] Y. Sato, M. Nakamoto, Y. Tamaki, T. Sasama, I. Sakita, Y. Nakajima, M. Monden, and S. Tamura, "Image guidance of breast cancer surgery using 3-D ultrasound images and augmented reality visualization," *IEEE Trans. Med. Imag.*, vol. 17, no. 5, pp. 681–693, Oct. 1998.

[21] J. N. Welch, J. A. Johnson, M. Bax, R. Badr, and R. Shahidi, "A real-time freehand 3D ultrasound system for image-guided surgery," in *Proc. IEEE Ultrason. Symp.*, San Juan, Puerto Rico, 2000, pp. 1601–1604.

[22] F. Lindseth, G. A. Tangen, T. Langø, and J. Bang, "Probe calibration for freehand 3-D ultrasound," *Ultrasound Med. Biol.*, vol. 29, pp. 1607–1623, Nov. 2003.

[23] R. C. Gonzalez and R. E. Woods, *Digital Image Process*, 2nd ed. Englewood Cliffs, NJ: Prentice-Hall, 2002.

[24] E. R. Davies, *Machine Vision: Theory, Algorithms, Practicalities*, 3rd ed. San Mateo, CA: Morgan Kaufmann, 2005.

[25] D. D. Frantz, A. D. Wiles, S. E. Leis, and S. R. Kirsch, "Accuracy assessment protocols for electromagnetic tracking systems," *Phys. Med. Biol.*, vol. 48, pp. 2241–2251, 2003.

[26] J. F. Cai, Z. Luo, L. Gu, R. Xu, and Q. Zhao, "The implementation of an integrated computer-assisted system for minimally invasive cardiac surgery," *Int. J. Med. Robot. Comput. Assisted Surg.*, vol. 6, pp. 102–112, 2010.

[27] N. Li, T. Beck, J. Chen, C. Biermann, L. Guo, H. Sun, F. Gao, and C. Liu, "Assessment of thoracic aortic elasticity: A preliminary study using electrocardiographically gated dual-source CT," *Eur. Radiol.*, vol. 21, pp. 1564–1572, Feb. 2011.

[28] D. Marciniak and C. E. Smith, "Pros and cons of transesophageal echocardiography in trauma care," *Internet J. Anesthesiol.*, vol. 23, no. 2, 2010.

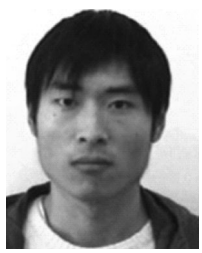

Zhe Luo received the Eng. Master's degree in software engineering from Shanghai Jiao Tong University, Shanghai, China, in 2010, where he is currently working toward the Ph.D. degree in biomedical engineering at the School of Biomedical Engineering.

His current research interests include computer-assisted surgery, medical image processing, and computer graphics.

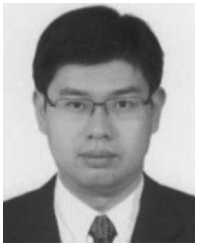

Junfeng Cai received the Med. Master's degree in medicine cardiosurgery from Shanghai Medical College, Fudan University, Shanghai, China, in 2007.

After completing the MD degree, he was with Zhongshan Hospital. Since 2009, he has been with Ruijin Hospital, Shanghai Jiao Tong University, Shanghai, where he is currently an Attending Doctor in the Department of Cardiosurgery. His research experiences includes complete myocardium reconstruction and revascularization using Omentum combined laser, preoperative planning of robotic cardiac surgery, and surgical navigation.

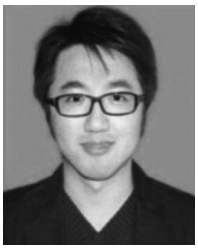

Su Wang received the Bachelor's of Medicine degree from Anhui Medical University, Anhui, China, in 2009. He is currently working toward the Master's degree in medicine cardiosurgery at the School of Medicine, Ruijin Hospital, Shanghai Jiao Tong University, Shanghai, China.

His research interests include surgical navigation and robotic surgery.

Qiang Zhao received the MD degree in surgery from Shanghai Medical College, Shanghai, China, in 1991.

He was with the Heart Institute of Saint Vincent Medical Center, Los Angeles, CA, from 1995 to 1998. He was with the Department of Cardiac Surgery, Zhongshan Hospital, Shanghai, from 1998 to 2009. He is currently the Director of the Department of Cardiosurgery, Ruijin Hospital, Shanghai Jiao Tong University, Shanghai. He has extensive clinical experience in the treatment of coronary heart disease, heart valves, congenital heart disease, high blood, heart transplant surgery, and other cardiovascular diseases. He completed nearly 10 000 cases of coronary artery bypass surgery. He has published more than 110 papers. His research interest include coronary heart surgery, minimally invasive and robot-assisted heart surgery, stem cell and genetic tissue engineering applications in cardiovascular disease, heart failure, and other aspects.

Dr. Zhao is a Standing Committee Member of Cardiovascular Surgery Branch of Chinese Medical Association, an American Society of Thoracic and Cardiovascular Surgery Member.

Terry M. Peters (F'09) received the Ph.D. degree in electrical engineering from the University of Canterbury, Christchurch, New Zealand, in 1974.

He is currently a Scientist in the Imaging Research Laboratories at the Robarts Research Institute, London, ON, Canada, and a Professor in the Departments of Medical Imaging and Medical Biophysics at the University of Western Ontario, ON, as well as a member of the Graduate Programs in Neurosciences and Biomedical Engineering. He is also an Adjunct Professor at McGill University, Montreal, Canada. He has authored more than 200 peer-reviewed papers and book chapters, a similar number of abstracts, and has delivered more than 180 invited presentations.

He is a Fellow of the Canadian College of Physicists in Medicine; the American Association of Physicists in Medicine, the Australasian College of Physical Scientists and Engineers in Medicine, the Medical Image Computing and Computer-Assisted Intervention (MICCAI) Society, and the Institute of Physics. He has been an Executive Member of the board of the MICCAI society, as well as its Treasurer. He has mentored more than 80 trainees at the Masters, Doctoral, and Postdoctoral levels. He was awarded the Erskine Travelling Fellowship by the University of Canterbury in New Zealand, in 1996 and again in 2010.

Lixu Gu (SM'11) received the Ph.D. degree in computer science from the Toyohashi University of Technology, Toyohashi, Japan, in 1999.

He was with Robarts Research Institute, ON, Canada, for three years, where he was responsible for the research and software development of the medical image analysis. In 2003, he moved to Shanghai to join the Research Group in Computer Science of Shanghai Jiao Tong University, Shanghai, China, where he is a Professor in the Department of Computer Science and School of Biomedical Engineering. At Shanghai Jiao Tong University, he founded the Laboratory of Image Guided Surgery and Therapy, where he is currently the Director. His research interests include pattern recognition, computer vision, medical image processing, computer graphics, virtual reality, image guided surgery and therapy. He is the author of more than 100 papers on related research area.

Dr. Gu is the Social Chair, and the PC Member of the 27th IEEE Engineering in Medicine and Biology Society Conference in Shanghai. He received the Best Poster in the 17th Congress of Computer Assisted Radiology and Surgery (CARS) in London, U.K., in 2003, and serves as the Program Committee Member of the CARS. He serves as an Associate Editor for both the IEEE TRANSACTIONS ON INFORMATION TECHNOLOGY IN BIOMEDICINE and the *International Journal of Computer Assisted Radiology and Surgery.*